LETTER • OPEN ACCESS

Physical coupling between inertial clustering and relative velocity in a polydisperse droplet field with background turbulence

To cite this article: M. Shyam Kumar *et al* 2023 *EPL* **142** 23002

A Letters Journal Exploring the Frontiers of Physics

April 2023

EPL, **142** (2023) 23002
doi: 10.1209/0295-5075/accbe7

www.epljournal.org

Physical coupling between inertial clustering and relative velocity in a polydisperse droplet field with background turbulence

M. Shyam Kumar[1(a)], S. R. Chakravarthy[2] and Manikandan Mathur[2,3]

[1] *Department of Mechanical Engineering, University of Minnesota - Minneapolis, MN 55455, USA*
[2] *Department of Aerospace Engineering, Indian Institute of Technology Madras - Chennai, 600036, India*
[3] *Geophysical Flows Lab, Indian Institute of Technology Madras - Chennai, 600036, India*

received 7 November 2022; accepted in final form 11 April 2023
published online 24 April 2023

Abstract – Natural processes, ranging from blood transport to planetary formation, are strongly influenced by particle collisions induced by background turbulence. While inertial clustering and particle pair relative velocity are recognized as the main collision enhancement factors, their physical coupling is poorly understood. In this experimental study, we measure clustering and relative velocity in a polydisperse droplet field with background air turbulence, to directly demonstrate the physical coupling between these collision enhancement factors. This coupling is shown to cause an inverse relation between clustering and relative velocity in the mean-flow–dominated turbulent flow we study, thus suppressing the intuitive effect of an increase in droplet collision rate with background air turbulence. Turbulence modulation due to clustering, and the resultant reduction of caustic droplet pairs with large relative velocities, are found to be the key physical mechanisms, and should be a consideration in droplet collision rate estimates in warm rain initiation.

Introduction. – Droplet collisions and subsequent coalescence in a turbulent air flow are of significant importance for a wide range of natural and industrial applications. For example, turbulence-driven droplet coalescence is thought to be an important driving mechanism for warm rain initiation [1–3]. On the other hand, the lack of mixing associated with fuel droplet coalescence is detrimental for combustion engines [4]. The collision rates in a turbulent flow depend on two factors: i) preferential concentration/clustering of droplets, and ii) relative velocity between nearby droplets. Theoretical estimates of collision rates have highlighted the role of these two factors [5], which in turn have motivated several studies on relevant physical mechanisms [6–11]. While a centrifugal mechanism regulates preferential concentration for Stokes number $St \approx 1$ [3], the sweep-stick mechanism plays a vital role in $St < 1$ and $St > 1$ droplet clustering [12]. In regard to relative velocity, sling effect [13], caustics [14] and differential settling [15] are three commonly discussed mechanisms associated with turbulence.

While most of the aforementioned studies have focused on either clustering or relative velocity in isolation, the two factors are actually physically coupled [16]. For example, at small St, droplets undergoing a net inward drift (negative relative velocity) contribute to clustering [17]. In addition, the increase in local droplet volume fraction associated with clustering can affect the air flow turbulent length scales [18], which in turn influences the droplet relative velocities. Apart from the assumption of no turbulence modulations by droplets, most previous studies have also been performed in either monodisperse [2] or bidisperse [16,19] droplet fields. In realistic droplet fields, however, a relatively wide range of droplet sizes (and hence a wide range of St too) occur, and the combined effect of different droplet classes on collision rates must be taken into account [8].

A recent experimental study reported that there exists an optimum background turbulent intensity for which polydisperse droplet size growth rate is maximized [20]. A follow-up study then highlighted how different size classes of droplet pairs primarily contribute to collisions at different turbulent intensities [21]. These studies fell short

(a) E-mail: shyamkuttamath@gmail.com (corresponding author)

of identifying the underlying physical mechanisms, which in turn would influence the physical coupling between the collision enhancement factors. To investigate the physical coupling, rigorous and independent quantitative measurements of clustering and relative velocity are needed, which was not attempted in either of the aforementioned studies [20,21]. In this paper, we advance the experimental methodology and analysis used in [20,21] to demonstrate and understand the physical interaction between clustering and relative velocity in a polydisperse droplet field, the relatively less addressed turbulence modulation, and finally investigate their influence on collision rates. The dynamical regimes explored in our experiments are not easily accessed in numerical simulations due to the difficulties associated with combining Lagrangian and Eulerian frameworks [22]. Specifically, we use a novel combination of phase Doppler interferometry (PDI), long distance microscopy (LDM) and 3D tomographic particle imaging to independently measure clustering and relative velocity in a polydisperse droplet field in air flows of different turbulent intensities.

Experimental methodology. – A vertically oriented air flow facility along with an active turbulence generator (ATG) is used to produce a flow of a desired turbulent intensity I. The ATG consists of rotating vanes driven by an array of externally controlled mutually perpendicular rods in a 270 mm × 270 mm square box [23]. The turbulent intensity imparted to a given air flow of mean velocity U is controlled using the maximum rotational speed ω of the vanes. Polydisperse water droplets in the size range 0–120 μm are introduced using a pressure swirl atomizer placed just downstream of the ATG. This experimental set-up has been used in two previous studies [20,21], and more details (including a schematic in fig. S1 in the Supplementary Material `Supplementarymaterial.pdf` (SM)) are provided in sect. 1 of the SM.

Fourteen different values of I are realized by appropriately changing U and ω (see table 1). In the absence of the droplet field, the single phase turbulence characteristics of the background air flow were quantified using Laser Doppler Velocimetry (LDV). The air flow turbulence can get modified in the presence of a droplet field, which we measure using PDI. Specifically, a turbulent intensity I_{PDI} is estimated in the experiments with the droplet field, by conditionally sampling only the sufficiently small droplets (diameter $d_i < 10\,\mu$m) that are likely to faithfully follow the local flow. For different I, St corresponding to $d_i = 10\,\mu$m is in the range 0.04–0.25. With $St < 1$ for all the droplets with $d_i < 10\,\mu$m across all the flow conditions, it is reasonable to consider these droplets to estimate I_{PDI}. More details of the experimental characterization of the turbulent air flow and the droplet field are provided in [20].

The temporal evolution of droplet size distribution is used to quantify droplet size growth in turbulent flows [24]. The mean droplet diameter and the mean droplet axial (along the gravity direction, denoted as x) velocity are measured at different axial and lateral locations (denoted as y). At each point, the mean droplet diameter d_m and axial velocity u_m are estimated by averaging individual droplet diameter d_i and axial velocity u_i of 30000 droplet acquisitions in PDI. Measurements are taken far downstream from the nozzle exit ($200 \leq x \leq 400$ mm, $-20 \leq y \leq 20$ mm), where the variation in d_m and u_m along the lateral direction is minimal. d_m is further averaged across different lateral locations to obtain D_m at each axial location, which is associated with a corresponding droplet residence time t_r since the entry into the measurement region.

Table 1: Turbulent intensity (I/I_{PDI}), the Kolmogorov length scale (η) and the corresponding Kolmogorov velocity (u_η) achieved by varying the mean axial air velocity U just upstream of the ATG and the maximum rotational speed ω of the ATG vanes. η and u_η are estimated from the particle-free flow experiments.

No.	U (m/s)	ω (rpm)	I/I_{PDI} (%)	η (μm)	u_η (m/s)
1	0.44	300	8.5/8.3	329	0.0456
2	0.44	750	9.1/8.9	315	0.0476
3	0.66	300	9.5/9.0	310	0.0484
4	0.66	750	10.0/9.6	303	0.0495
5	0.77	0	10.4/10.0	251	0.0598
6	0.82	0	10.5/10.3	232	0.0647
7	0.77	300	10.7/10.4	222	0.0676
8	0.77	750	11.4/11.0	210	0.0714
9	0.88	750	11.5/11.3	201	0.0746
10	1.30	0	12.2/12.3	168	0.0893
11	1.30	150	12.9/13.1	150	0.1000
12	1.30	750	14.2/14.7	160	0.0938
13	1.73	0	15.2/15.4	148	0.1014
14	1.73	1125	15.8/16.1	132	0.1136

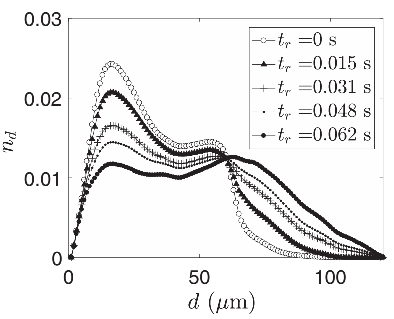

Fig. 1: Variation in droplet size distribution with residence time t_r for the flow condition with $I = 11.5\%$ (exp. no. 9 in table 1).

In fig. 1, the variation of the normalized droplet size distribution (estimated from measured droplet sizes across all transverse locations at a fixed axial location) with residence time t_r in the experiment with $I = 11.5\%$ is shown.

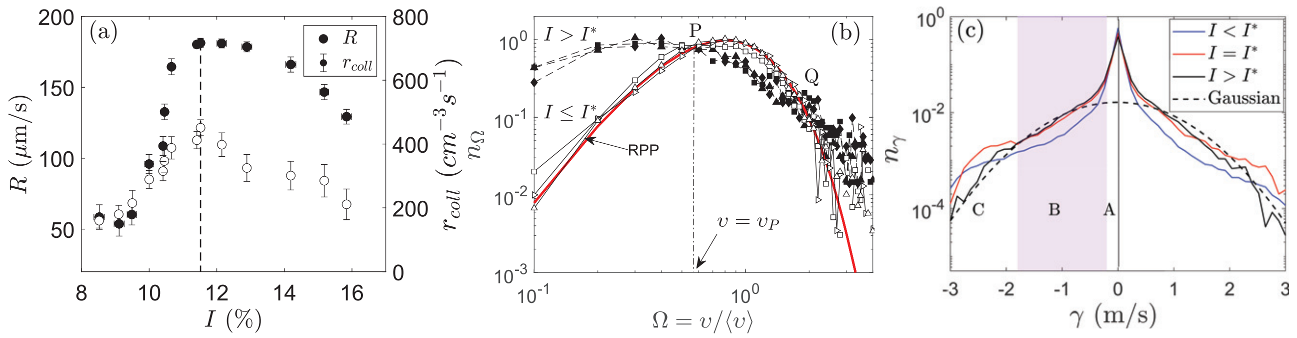

Fig. 2: Measurements of droplet collision rates, and the two collision rate enhancement factors, namely clustering and relative velocity. (a) Droplet size growth rate R (filled circles) plotted as a function of turbulent intensity I based on the experiments listed in table 1. Corresponding collision rate r_{coll} estimates based on LDM measurements are shown as unfilled circles. (b) PDF of the normalized Voronoï cell volume ($\Omega = v/\langle v \rangle$) for different values of I. Open and filled markers correspond to $I \leq I^*$ and $I > I^*$, respectively. The red solid line represents the distribution of Ω if particles are spatially distributed according to a random Poisson process (RPP). (c) PDFs of droplet pair lateral relative velocity for three different turbulent intensities. The black dashed line corresponds to the Gaussian distribution.

The droplet residence time between two nearby axial locations x_1 and x_2 is estimated as $2(x_2 - x_1)/[U_m(x_1) + U_m(x_2)]$, where $U_m(x)$ is the laterally averaged mean droplet axial velocity at the axial location x. These estimates are then cumulatively added over multiple axial location pairs to obtain the residence time t_r between the entry to the measurement region and the current location. With an increase in t_r, the fractions of relatively small and large droplets decrease and increase, respectively. Correspondingly, the mean droplet diameter D_m increases from $28\,\mu$m at $t_r = 0\,$s to $41\,\mu$m at $t_r = 0.062\,$s. In our experiments, measurements at increasing axial locations are equivalent to droplet field measurements at increasing droplet residence times.

The rate of increase of D_m with t_r, which is a clear indication of droplet coalescence, varies with the air turbulent intensity I. The droplet size growth rate R is estimated as $R = \mathrm{d}D_m/\mathrm{d}t_r$ at different I, and plotted in fig. 2(a). An optimum turbulent intensity of $I = 11.5\%$ for the maximum droplet size growth is observed. This observed trend in R *vs.* I was understood in terms of collision rate estimates in [20]. The droplet collision rate r_{coll} over the measurement region was estimated using LDM [20]. Specifically, LDM was used to capture several individual droplet collision events over a 4.5 mm × 4.5 mm region to subsequently estimate r_{coll}. Figure 2(a) shows that r_{coll} follows a similar trend as R when plotted against I, with the same optimum I ($I^* = 11.5\%$) at which R and r_{coll} are maximum.

With respect to the role of gravity, the number of collisions caused by relative settling between differently sized droplets can be quantified using the non-dimensional Froude number $Fr = \nu^2/(g\eta^3)$; it represents the importance of gravitation relative to the acceleration caused by the turbulent flow [25]. Across the 14 different flow conditions, Fr increases monotonically with I, with an average Fr of ≈ 2 and 6 for the flow conditions $I \leq I^*$ and $I > I^*$, respectively. In other words, with an increase in I, the importance of gravity reduces and this in turn could reduce the number of collisions caused by relative settling. Furthermore, for $Fr > 1$, the trend in velocity difference statistics with St is invariant with Fr [25]; therefore, it indicates a possibly weak effect of gravity across all the flow conditions considered in our study.

Droplet clustering is quantified using Voronoï tessellation, which is the mapping of space into Voronoï cells; the Voronoï cell of a given droplet comprises all the points which are closer to the droplet than to any other droplets [26,27]. The Voronoï cell volume v is inversely proportional to the local number density, and its probability distribution function (PDF) has previously been used to detect and characterize particle clustering [8,28]. Here, we perform a Voronoï analysis on droplet spatial coordinates (in 3D) obtained from tomographic imaging, the details of which are given in the SM (sect. 2). The Voronoï analysis is carried out using the open source visualization tool OVITO [29].

PDFs of the normalized Voronoï cell volume $\Omega = v/\langle v \rangle$ for different I are shown in fig. 2(b), where $\langle v \rangle$ is the mean of v. The spatial distribution of unclustered particles could be modeled as a random Poisson process (RPP), and the corresponding PDF of Ω is described by a Gamma function [28], shown by the red solid curve in fig. 2(b). The PDFs of Ω corresponding to flow conditions with turbulent intensity $I \leq I^*$ (unfilled symbols in fig. 2(b)) closely follow the Gamma function (except at large Ω, which is anyway susceptible to non-negligible errors in the Voronoï analysis), thereby indicating that clustering is not prominent for $I \leq I^*$. In contrast, substantial deviation from the Gamma function is observed for cases with $I > I^*$ (filled symbols). Specifically, relatively small values of Ω are observed to be significantly more likely than for RPP, suggesting that clustering is prevalent for $I > I^*$.

For $I > I^*$, the PDFs follow a non-RPP trend at all Ω, and cross the RPP PDF at two points (marked as P and Q in fig. 2(b)). The points P and Q correspond to Voronoï cell volumes of υ_P and υ_Q, respectively, which are measures of the largest cluster size and the smallest void size. Observing that υ_P is about $(10\eta)^3$, where η is the turbulent dissipative length scale, we conclude that the clustering length scale is $\approx 10\eta$. In other words, clustering in the $I > I^*$ experiments is inertial, and not sub-Kolmogorov. This implies that the droplet clustering is substantially influenced by a wide range of turbulent length scales, and not just by the dissipative length scale. As a result, the velocity distribution of all the droplets is likely influenced, which in turn, potentially alters the droplet relative velocity statistics. Hence, we proceed with an independent statistical estimation of the droplet relative velocities, which is considered as a prominent collision enhancement factor alongside clustering.

From the LDM-based droplet tracking, the relative velocity of a pair droplets is estimated as $\gamma(r) = (\mathbf{v}_1 - \mathbf{v}_2) \cdot \mathbf{r}/|\mathbf{r}|$, where $\mathbf{v}_1$, $\mathbf{v}_2$ are the droplet velocities, $\mathbf{r}$ is the separation vector that goes from droplet 2 to 1 and $r = |\mathbf{r}|$ [21,30]. $\gamma(r) < 0$ and $\gamma(r) > 0$ imply that the droplets are moving towards and away from each other, respectively. With D_1 and D_2 denoting the diameters of large and small droplets within each droplet pair, we use D_1/D_2 as a measure of droplet size difference within a pair. At very large r, say much larger than the clustering length scale of 10η, the droplet pair relative velocity is expected to be equivalent to the relative velocity between fluid tracers separated by the same r [31]. To investigate the coupling between clustering and relative velocity, we therefore choose a value of $r = 10\eta$, which also happens to be an estimate of the dissipation range in homogeneous isotropic turbulence [31]. It is possible to consider $r \neq 10\eta$ too, though the exact value we choose within $3\eta \leq r \leq 20\eta$ does not influence our final conclusions (see sect. 3 of the SM).

Figure 2(c) shows the distribution of γ at different turbulent intensities. The distribution of γ has been extensively studied analytically [31–33] as well as experimentally [30] in monodisperse and bidisperse droplet fields. Pan and Padoan [32] have shown that exponential and Gaussian distributions describe the γ distribution for small and large St particle pairs, with identical particles, respectively. In bidisperse droplet fields with small and large St droplets, a Gaussian distribution is again found to describe the γ distribution [33]. To the best of our knowledge, a systematic study of relative velocity distributions in a polydisperse droplet field has not been previously reported. For each of $I < I^*$, $I = I^*$ and $I > I^*$ (cases 1, 9 and 12 in table 1), the γ distribution n_γ shows a similar non-Gaussian peak at $\gamma = 0$, displaying an exponential-like decay as $|\gamma|$ is increased. Interestingly, the $I < I^*$ case (no clustering) deviates from the other two cases at around $|\gamma| = 0.2$ m/s, indicated by the boundary between regions A and B.

In region A, the relative velocities are small, and hence the corresponding droplet pairs are unlikely to collide. We find the average value of D_1/D_2 of all the droplet pairs in region A to be close to unity, with a relatively small St ($St < 0.8$) for the corresponding droplets. This suggests that small St nearly monodisperse regime is at play here, for which an exponential distribution for γ has been reported [32,33]. In other words, region A comprises what are known as correlated continuous droplet pairs [21,32].

In region B, *i.e.*, -1.8 m/s $< \gamma < -0.2$ m/s, n_γ in all the three cases follow a similar trend, but with some key differences. While n_γ for $I < I^*$ continues to follow an exponential distribution in region B, the distributions for $I = I^*$ and $I > I^*$ have now switched over to a nearly Gaussian distribution. Furthermore, n_γ for $I = I^*$ and $I > I^*$ nearly overlap in region B, much like they do in region A. In region B, where the relative velocities are moderate and hence contributing more to collisions than region A, the average values of D_1/D_2 are 1.76, 1.98 and 1.81 for $I < I^*$, $I = I^*$ and $I > I^*$, respectively. Thus, region B comprises different-sized droplets within pairs, the occurrence of which is made possible by the polydispersity of the droplet field. The significantly larger overall collision rate at $I = I^*$ compared to $I > I^*$ (fig. 2(a)), however, cannot be attributed to region B since the corresponding relative velocity distributions are quite similar (fig. 2(c)).

At around $\gamma = -1.8$ m/s, marked as the boundary between regions B and C, n_γ for $I = I^*$ and $I > I^*$ begin to noticeably deviate from their behaviour in region B as γ is decreased. The distribution for $I < I^*$, however, does not deviate as much from its trend in region B. In region C, which corresponds to large relative velocities and hence a high likelihood of collisions, $I = I^*$ clearly has a larger number of occurrences than $I > I^*$. Owing to the similar distributions in regions A and B for $I = I^*$ and $I > I^*$, we conclude that region C is predominantly responsible for the observed trend of monotonic decrease of overall collision rate for $I > I^*$. The average value of D_1/D_2 in region C is 3.42 and 3.25 for $I = I^*$ and $I > I^*$, with such large values corresponding to caustic pairs [32,33], which are known to have large relative velocities even at small separation distances [2]. We proceed to directly plot the coupling between clustering and relative velocity by estimating their respective measures at different values of I.

As a quantitative measure of clustering, we define $\bar{A}_\Omega$ as the area under the distribution curve for Ω in the region to the left of point P (see fig. 2(b)), normalized by the corresponding area under the γ distribution. We recall that clustering leads to increased likelihood of small Voronoï volumes, thus increasing the area of the Ω distribution curve to the left of point P. Similarly, we define a relative velocity measure $\bar{A}_\gamma$ as the area under the γ distribution in region C (see fig. 2(c)), normalized by the corresponding area for a Gaussian distribution that fits the $I > I^*$ distribution in regions B and C. On the $\bar{A}_\Omega$-$\bar{A}_\gamma$ plane, the non-clustering and clustering regimes are clearly separated (fig. 3). In the non-clustering $I \leq I^*$ regime, $\bar{A}_\gamma$ rapidly increases with I (see inset of fig. 3). An increase in the

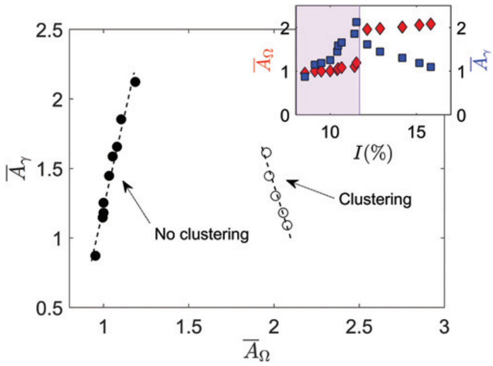

Fig. 3: Inverse relation between clustering and relative velocity. Variation of $\bar{A}_\gamma$ with $\bar{A}_\Omega$ for the 14 different turbulent intensities. Non-clustering ($I \leq I^*$) and clustering ($I > I^*$) flow conditions are shown using filled circle and unfilled circles, respectively. Variations of $\bar{A}_\Omega$ with I (red symbols) and $\bar{A}_\gamma$ with I (blue symbols) are shown in the inset.

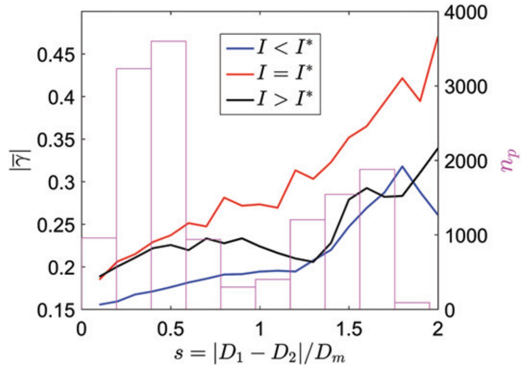

Fig. 4: Variation of the mean relative velocity magnitude $\overline{|\gamma|}$ with s for three different turbulent intensities. Distribution (see n_p on the right-hand side axis) of $s = |D_1 - D_2|/D_m$ in the $I = I^*$ experiment is shown using the histogram in the background.

likelihood of large relative velocities increases the likelihood of small Voronoï volumes, thus resulting in a small increase in $\bar{A}_\Omega$ with I for $I \leq I^*$ even though no clustering occurs in this regime. As soon as clustering sets in, $\bar{A}_\Omega$ expectedly increases abruptly; the corresponding abrupt decrease in $\bar{A}_\gamma$ represents the first reported direct evidence for coupling between clustering and relative velocity. A further increase in $\bar{A}_\Omega$ in the clustering regime results in further reduction in $\bar{A}_\gamma$, thus showing a trend that is opposite of what is observed in the non-clustering regime. In the clustering regime, the observed increase (decrease) in $\bar{A}_\Omega$ ($\bar{A}_\gamma$) is relatively small (large), which can be attributed to the clustering (relative velocity) measure being based on bulk (individual pairs) properties. In summary, while an increase in relative velocity, *i.e.*, $\bar{A}_\gamma$, results in a small increase of the clustering measure $\bar{A}_\Omega$ in the non-clustering regime, an increase in clustering results in a decrease in relative velocity in the clustering regime. In other words, relative velocity and clustering are physically coupled.

To further understand the mechanisms underlying the physical coupling between clustering and relative velocity, we first estimate the distribution of $s = |D_1 - D_2|/D_m$, where $D_m = (D_1 + D_2)/2$ is the mean droplet diameter within a pair. Small and large values of s correspond to continuous (similar-sized small droplets) and caustic (droplets of disparate sizes) droplet pairs, respectively [21]. Specifically, as shown using the histogram in fig. 4, the distribution of s for $I = I^*$ displays a bi-modal behaviour, with $s \approx 0.8$ separating the continuous and caustic pairs. Though not shown here, the corresponding distributions for $I < I^*$ and $I > I^*$ are found to be similar to that for $I = I^*$. The similarity in the distributions of s for different turbulent intensities suggests that the differences in the distribution curves for γ (fig. 2(c)) are probably due to changes in γ at each bin of s. Thus, we proceed to plot the mean relative velocity magnitude $\overline{|\gamma|}$ as a function of s for different values of I.

As expected, $\overline{|\gamma|}$ monotonically increases with s for all three values of I (case 3, case 9, case 12 in table 1) shown in fig. 4, indicating that caustic pairs tend to have a larger relative velocity than continuous pairs on an average. Increasing I from $I < I^*$ to $I = I^*$, a clear increase in $\overline{|\gamma|}$ is observed at each s. The increase in the caustic pairs region specifically contributes to increased likelihood of larger relative velocities (fig. 2(c)), and hence larger collision rates (fig. 2(a)) for $I = I^*$. We attribute the increase (with I) in relative velocities for $s > 0.8$ to the decrease in the Kolmogorov length scale η (increase in u_η) with I in the non-clustering regime (see table 1). Physically, a decrease in η results in a stronger influence of small-scale eddies on small droplets. Such a physical understanding is consistent with previous studies [32] reporting that relative velocities in caustic pairs are strongly dependent on the small scales.

In the clustering regime, an increase in I results in a decrease in $\overline{|\gamma|}$ at large s (fig. 4), which in turn reduces the likelihood of droplet pairs with a large relative velocity (as noted earlier from fig. 2(c)). While η continues to decrease (increase in u_η) with I in the clustering regime (see table 1), the onset of clustering seems to play a dominant role in reducing the relative velocities in caustic pairs. In other words, the energy in the small scales seems to be decreasing with I despite an increase in u_η. An evidence for such a trend is seen in the $I_{PDI} > I$ signature in the clustering regime (see table 1). The trend of enhanced turbulent intensity (compared to the particle-free flow) after clustering sets in indicates that clustering energizes the large scales [34]. This energization of large scales is likely to be an energy sink for the dissipative small scales, which then explains why the relative velocity magnitude in caustics pairs reduces with clustering. In addition, in the clustering regime, the distribution of γ is symmetric about $\gamma = 0$ (see fig. 2(c)), and a Gaussian distribution describes the caustic pairs (region C in fig. 2(c)) well. An implication of these observations is that both approaching and separating droplet pairs are influenced mainly by a common large length scale [31], which cannot impart a large relative velocity. A future study focused on the effects of clustering on the large scales of the flow would be worthwhile.

In conclusion, the presence of a physical coupling between inertial clustering and relative velocity, and its role in reducing droplet collision rates in a polydisperse droplet field with a mean-flow–dominated background air turbulence has been demonstrated in this experimental study. The reduction in collision rates upon clustering is shown to be strongly associated with the reduction of droplet pairs with large relative velocities, which in turn is physically coupled with the redistribution of energy to different turbulent length scales due to inertial clustering. Such an energy redistribution is evident in the turbulence modulation induced by the droplets, and the relative velocity of caustic pairs being well described by a Gaussian distribution. Our results and inferences highlight the importance of coupling between clustering and relative velocity, and also demonstrate how collision rates are non-trivially affected as a consequence. Incorporating this coupling in collision rate models of various fidelities remains a challenge, and should be a necessary consideration to understand warm rain initiation. Finally, it would be worthwhile to investigate the relevance of our conclusions to flow regimes that occur in other physical settings such as warm rain initiation, planetary disk formation, sand dunes, pneumatic transports and spray combustions in jet engines.

* * *

The authors acknowledge Jason Picardo for his critical reading of the manuscript.

Data availability statement: All data that support the findings of this study are included within the article (and any supplementary files).

REFERENCES

[1] Falkovich G., Fouxon A. and Stepanov M., *Nature (London)*, **419** (2002) 151.

[2] Wilkinson M., Mehlig B. and Bezuglyy V., *Phys. Rev. Lett.*, **97** (2006) 048501.

[3] Bec J., Biferale L., Boffetta G., Celani A., Cencini M., Lanotte A., Musacchio S. and Toschi F., *J. Fluid Mech.*, **550** (2006) 349.

[4] Kuo K. K., (1986).

[5] Sundaram S. and Collins L. R., *J. Fluid Mech.*, **335** (1997) 75.

[6] Reade W. C. and Collins L. R., *Phys. Fluids*, **12** (2000) 2530.

[7] Bec J., Celani A., Cencini M. and Musacchio S., *Phys. Fluids*, **17** (2005) 073301.

[8] Sumbekova S., Cartellier A., Aliseda A. and Bourgoin M., *Phys. Rev. Fluids*, **2** (2017) 024302.

[9] Squires K. D. and Eaton J. K., *J. Fluid Mech.*, **226** (1991) 1.

[10] Eaton J. K. and Fessler J., *Int. J. Multiphase Flow*, **20** (1994) 169.

[11] Jacobs C. N., Merchant W., Jendrassak M., Limpasuvan V., Gurka R. and Hackett E. E., *PLoS ONE*, **11** (2016) e0159645.

[12] Goto S. and Vassilicos J., *Phys. Rev. Lett.*, **100** (2008) 054503.

[13] Bewley G. P., Saw E.-W. and Bodenschatz E., *New J. Phys.*, **15** (2013) 083051.

[14] Devenish B., Bartello P., Brenguier J.-L., Collins L., Grabowski W., IJzermans R., Malinowski S., Reeks M., Vassilicos J., Wang L.-P. *et al.*, *Q. J. R. Meteorol. Soc.*, **138** (2012) 1401.

[15] Good G., Ireland P., Bewley G., Bodenschatz E., Collins L. and Warhaft Z., *J. Fluid Mech.*, **759** (2014) R3.

[16] Bec J., Biferale L., Cencini M., Lanotte A. and Toschi F., *J. Fluid Mech.*, **646** (2010) 527.

[17] Chun J., Koch D. L., Rani S. L., Ahluwalia A. and Collins L. R., *J. Fluid Mech.*, **536** (2005) 219.

[18] Grabowski W. W. and Wang L.-P., *Annu. Rev. Fluid Mech.*, **45** (2013) 293.

[19] Bec J., *Phys. Fluids*, **15** (2003) L81.

[20] Kumar M. S., Chakravarthy S. and Mathur M., *Phys. Rev. Fluids*, **4** (2019) 074607.

[21] Kumar M. S., Mathur M. and Chakravarthy S., *J. Fluid Mech.*, **917** (2021) A12.

[22] Vreman B., Geurts B. J., Deen N., Kuipers J. and Kuerten J. G., *Flow, Turb. Combust.*, **82** (2009) 47.

[23] Mulla I., Sampath R. and Chakravarthy S., *Heat Mass Transf.*, **55** (2019) 1887.

[24] Shaw R. A., *Annu. Rev. Fluid Mech.*, **35** (2003) 183.

[25] Bec J., Homann H. and Ray S. S., *Phys. Rev. Lett.*, **112** (2014) 184501.

[26] Monchaux R., Bourgoin M. and Cartellier A., *Phys. Fluids*, **22** (2010) 103304.

[27] Monchaux R., *New J. Phys.*, **14** (2012) 095013.

[28] Tagawa Y., Mercado J. M., Prakash V. N., Calzavarini E., Sun C. and Lohse D., *J. Fluid Mech.*, **693** (2012) 201.

[29] Stukowski A., *Modell. Simul. Mater. Sci. Eng.*, **18** (2009) 015012.

[30] Dou Z., Ireland P. J., Bragg A. D., Liang Z., Collins L. R. and Meng H., *Exp. Fluids*, **59** (2018) 30.

[31] Ireland P. J., Bragg A. D. and Collins L. R., *J. Fluid Mech.*, **796** (2016) 617.

[32] Pan L. and Padoan P., *Astrophys. J.*, **776** (2013) 12.

[33] Pan L., Padoan P. and Scalo J., *Astrophys. J.*, **791** (2014) 48.

[34] Petersen A. J., Baker L. and Coletti F., *J. Fluid Mech.*, **864** (2019) 925.